

# Crystal structures and proton dynamics in potassium and cesium hydrogen bistrifluoroacetate salts with strong symmetric hydrogen bonds

Alain Cousson

*Laboratoire Léon Brillouin (CEA-CNRS), C.E. Saclay, 91191 Gif-sur-Yvette  
cedex, France*

Juan F R Archilla

*Group of Nonlinear Physics, Departamento de Física Aplicada I, ETSI  
Informática. Avda Reina Mercedes s/n, 41012-Sevilla, Spain*

John Tomkinson

*Rutherford Appleton Laboratory, Chilton, Didcot, OX11 0QX, United Kingdom*

François Fillaux<sup>1</sup>

*LADIR-CNRS, UMR 7075 Université Pierre et Marie Curie, 2 rue Henry  
Dunant, 94320 Thiais, France*

---

<sup>1</sup> Corresponding author

homepage <http://ulyse.glv-t-cnrs.fr/ladir/pagefillaux.htm>

---

**Abstract**

The crystal structures of potassium and cesium bistrifluoroacetates were determined at room temperature and at 20 K and 14 K, respectively, with the single crystal neutron diffraction technique. The crystals belong to the  $I2/a$  and  $A2/a$  monoclinic space groups, respectively, and there is no visible phase transition. For both crystals, the trifluoroacetate entities form dimers linked by very short hydrogen bonds lying across a centre of inversion. Any proton disorder or double minimum potential can be rejected. The inelastic neutron scattering spectral profiles in the OH stretching region between 500 and 1000  $\text{cm}^{-1}$  previously published [Fillaux and Tomkinson, Chem. Phys. 158 (1991) 113] are reanalyzed. The best fitting potential has the major characteristics already reported for potassium hydrogen maleate [Fillaux *et al.* Chem. Phys. 244 (1999) 387]. It is composed of a narrow well containing the ground state and a shallow upper part corresponding to dissociation of the hydrogen bond.

*Key words:* Single crystals neutron diffraction, inelastic neutron scattering, hydrogen bond, proton dynamics

---

---

*Email addresses:* cousson@llb.saclay cea.fr (Alain Cousson), archilla@us.es (Juan F R Archilla), J.Tomkinson@rl.ac.uk (John Tomkinson), fillaux@glvt-cnrs.fr (François Fillaux).

## Introduction

In most of hydrogen bonds  $AH \cdots B$ , it is widely accepted that the potential energy for the motion of the hydrogen atom has two minima [1–5]. For symmetric systems  $A \cdots H \cdots A$ , the two wells can be equivalent and proton tunnelling may occur. For the shortest hydrogen bonds the distance between the two minima decreases and the potential barrier between them may disappear [6]. There remains a single well at the centre and such symmetric structures can be regarded as “intermediate-states” for proton transfer in chemical reactions or biological processes [7,8]. Our motivation for the studies of the title compounds reported below is to shed light on the potential function experienced by protons involved in strong symmetric hydrogen bonds.

A classic example of a symmetric intramolecular hydrogen bond is the mono-anion of maleic acid in potassium hydrogen maleate,  $KH(OOC-CH=CH-COO)$ . This extremely short  $O \cdots H \cdots O$  bond, with length  $R_{O \cdots O} = 2.437 \text{ \AA}$  and with the proton located at the centre, has been studied with different techniques: X-ray diffraction [9,10]; infrared and Raman [11–15] and inelastic neutron scattering (INS) [16–18]. More recently, the shape of the potential function for the proton motion along the hydrogen bond has been determined from neutron diffraction and INS spectra of single crystals at low temperature [19]. This potential is composed of a sharp well at the centre of the hydrogen bond and two secondary minima at  $\approx 1000 \text{ cm}^{-1}$  above the central minimum. These secondary minima are located at  $\approx \pm 0.8 \text{ \AA}$  from the centre. Upon the assumption that these secondary minima occur because the hydrogen bond geometry is no longer stable after excitation of the  $\nu$  OH mode above  $500 \text{ cm}^{-1}$ , it could be concluded that whilst the ground state wave function is “hydrogen-bonding” the excited vibrational states are “hydrogen-nonbonding”. The potential shape is a snapshot of the proton motion during the dissociation of the hydrogen bond upon excitation of the OH stretching mode. The apparent paradox of a modest dissociation energy threshold observed in one of the “strongest” known hydrogen bonds was ascribed to partial compensation of the energy of formation of the hydrogen bond by a strain energy arising from the planarity of the maleate ring. This potential function was criticized by Wilson *et al.* [20] on the basis of plane-wave DFT calculations. However, such calculations performed over a very limited range of proton displacement, corresponding to potential energy far below the ground state, are not conclusive [21].

So far, potassium hydrogen maleate is the only reported example we are aware of this unforeseen potential shape and whether this system is unique or if similar potentials also apply to other strong symmetric hydrogen bonds is an open question.

By contrast, a totally different potential shape has been proposed for potassium and cesium hydrogen bistrifluoroacetates,  $\text{KH}(\text{CF}_3\text{COO})_2$  and  $\text{CsH}(\text{CF}_3\text{COO})_2$ , which are also classic examples of strong and symmetric hydrogen bonds at room temperature [6] with lengths  $R_{\text{O}\cdots\text{O}} = 2.435$  and  $2.38$  Å, respectively [22]. The vibrational spectra of these salts have been thoroughly investigated [23,24]. Upon comparison of infrared, Raman and INS spectra, the vibrational modes for protons were assigned at  $\approx 800$   $\text{cm}^{-1}$  ( $\nu$  OH),  $1300$   $\text{cm}^{-1}$  ( $\gamma$  OH) and  $1600$   $\text{cm}^{-1}$  ( $\delta$  OH). For both systems, the  $\nu$  OH band profiles observed with INS and in the infrared are almost identical. They show complex multi-component profiles with main components at  $\approx 700$ ,  $800$  and  $880$   $\text{cm}^{-1}$  and weaker components in the range  $500$ - $1000$   $\text{cm}^{-1}$ . These profiles were regarded as mainly due to Evans-type [25,26] or Fano-type [27] interactions with internal modes of the  $\text{CF}_3\text{COO}$  entities. For the Cs derivative, a very sharp INS band at  $\approx 90$   $\text{cm}^{-1}$  was tentatively assigned to proton tunnelling along the OH stretching coordinate and an asymmetric double minimum potential was proposed, quite at variance to the case of potassium hydrogen maleate.

However, with hindsight, such a double well is rather unlikely for very short hydrogen bonds because the minima located at  $\approx \pm 0.5$  Å off centre (see Fig. 7 in Ref. [24]) are quite incompatible with the  $R_{\text{O}\cdots\text{O}}$  length. The O—H distance less than  $0.7$  Å is quite unrealistic. In addition, there is no evidence of  $\nu$  OH tunnelling transition for the K derivative, whereas band profiles, crystal structures and hydrogen bond lengths are very similar.

The localization of the proton in an asymmetric double well is also in conflict with the known crystal structures determined with X-ray diffraction [22]: hydrogen bonds are centrosymmetric for the two salts at room temperature. However, crystal structures at low temperature are unknown and a symmetry breakdown cannot be excluded. In order to determine the proton location we have used the single crystal neutron diffraction technique. The crystal structures of the two salts at  $20$  K or  $14$  K and at  $298$  K (room temperature) are presented below. In both systems, hydrogen bonds are symmetrical at any temperature, with protons clearly located at the centre. It is shown that potential functions largely inspired by that of potassium hydrogen maleate, though significantly different, account for the OH stretching INS band profiles.

## 1 Crystal structures

Single crystals were obtained by slow recrystallization from aqueous solutions. These very hygroscopic colorless crystals were handled under dry atmosphere. For neutron diffraction measurements, approximately cubic samples ( $3 \times 3 \times 3$   $\text{mm}^3$ ) were cut from large crystals and tested at room temperature. Samples were loaded into aluminum containers that were then mounted in a cryostat.

For measurements at low temperature, they were cooled down with a flow of helium vapor.

Measurements (see Table 1) were carried out on a Stoe four-circle diffractometer 5C2 at the Orphée reactor (Laboratoire Léon-Brillouin) [28]. The incident neutron wavelength was  $\lambda = 0.8305 \text{ \AA}$ . Absorption corrections were ignored. Data analysis was carried out with the computer package CRYSTALS [29]

Crystal structures at any temperature are similar to those previously determined with X-ray diffraction [22]. The potassium and cesium salts belong to the  $I2/a$  and  $A2/a$  monoclinic space groups, respectively, both with four entities in the unit cells (see Figs. 1 and 2). The two acetate residues are crystallographically equivalent for both salts. They are linked by short hydrogen bonds lying across a centre of inversion (see Figs. 3 and 4). Hydrogen bond lengths are identical at low temperature:  $R_{O\dots O} = 2.436(3)$  and  $2.436(4) \text{ \AA}$ , for the K and Cs derivatives, respectively (see Tables 3 and 6). At room temperature, they are slightly different:  $2.432(3)$  and  $2.444(2) \text{ \AA}$ , respectively. However, the difference is tiny compared to the thermal factors for O atoms ( $\approx 0.05 \text{ \AA}^2$ , see Tables 4 and 7).

At any temperature there is no evidence for splitting of the proton probability density that could be attributed to disorder over different sites or to a double well potential. At low temperature, the temperature factors for oxygen atoms are much smaller than those for protons. As the latter compare to the mean square amplitudes of displacements for proton oscillators with averaged frequencies of  $\approx 1000 \text{ cm}^{-1}$  (see Tables 4 and 7), they are primarily due to proton dynamics in a single well. At room temperature, the temperature factors increase substantially (see Figs. 3 and 4). For protons these factors can be regarded as combinations of the proton contribution, virtually unchanged compared to that at low temperature, with those of the oxygen atoms (those labelled O(2) in Tables 4 and 7), which increase dramatically. Therefore, even at room temperature, the temperature factors are not compatible with any realistic double well potential, with minima separated by more than  $0.5 \text{ \AA}$  [24].

Finally, trifluoroacetate entities have different conformations for the two salts (see Figs. 3 and 4). A C—F bond is *trans* with respect to the CO(H) bond for the K salt. One of the C—F bonds is virtually perpendicular to the carboxylic plane for the Cs derivative.

## 2 INS band profiles and proton dynamics

The  $(\text{CF}_3\text{COO}\cdots\text{H}\cdots\text{OOC}\text{CF}_3)^-$  entities occupying  $Ci$  sites, the OH stretching and bending modes are only infrared active ( $Au + Bu$ ) [23]. The stretching mode gives a broad continuum of intensity centered at  $\approx 800 \text{ cm}^{-1}$ , whereas bending modes are extremely weak and barely visible. This assignment scheme is corroborated by the correlation between  $\nu$  OH frequencies and hydrogen bond lengths,  $R_{\text{O}\cdots\text{O}}$  [6]. It is also consistent with the OH stretching at  $\approx 600 \text{ cm}^{-1}$  for the maleate salt [19].

In the crystal structures, the shortest distances between protons are 4.34 and  $6.72 \text{ \AA}^{-1}$  for K and Cs salts, respectively. These protons are further isolated by the stacking of  $\text{CF}_3$  entities and  $\text{K}^+$  or  $\text{Cs}^+$  ions. Dynamical coupling between protons is negligible. The great similarity of the  $\nu$  OH profiles observed in the infrared and with INS (free of symmetry related selection rule) confirms that crystal field splitting is not resolved [24]. Moreover, the profiles are almost identical for the two salts (see below), though they have different crystal structures. We can safely conclude that the  $Au - Bu$  splitting is negligible compared to the intrinsic width of the  $\nu$  OH profile.

The INS spectra in the OH stretching region, from Ref. [24], are presented in Fig. 5. The raw data have been reanalyzed with a better background treatment. The spectra, renormalized with respect to the amount of sample in the beam, show very similar intensities, as anticipated for these closely related salts. The OH stretching profiles were decomposed into gaussian components (see Tables 8 and 9) and a linear baseline was subtracted. The grey components correspond to Raman bands previously attributed to  $\delta$   $\text{CF}_3$  modes [24]. The remaining bands, for example at  $\approx 602$  (597), 704 (704), 799 (798), 871 (880) and 955 (950)  $\text{cm}^{-1}$  for the K (Cs) derivative, are attributed to the OH stretching modes.

As anticipated for hydrogen bonds with equal lengths, the  $\nu$  OH profiles are virtually identical. Only in the  $820\text{-}920 \text{ cm}^{-1}$  range, two components at 850 and  $870 \text{ cm}^{-1}$  are clearly visible for the Cs derivative, while there is only one component for the K analogue. As rather strong Raman bands were observed at 850 and  $854 \text{ cm}^{-1}$  for the potassium salt [24], we conclude that the INS component at  $870 \text{ cm}^{-1}$  for the K derivative is an unresolved comprise of  $\delta$   $\text{CF}_3$  and  $\nu$  OH modes (see Table 8 and 9). It sounds logical that different frequencies for the  $\delta$   $\text{CF}_3$  modes arise from different conformations of the  $\text{CF}_3$  groups (compare Figs. 3 and 4).

The rather complex  $\nu$  OH profiles are thus supposed to arise primarily from the internal dynamics of the hydrogen bond. At first sight, the slowly varying spacing of the components, namely  $\approx 102$  (107), 95 (94), 72 (82), 84 (70)

cm<sup>-1</sup> in Tables 8 and 9, suggests a Franck-Condon-like progression due to strong coupling with O···O modes [30–33]. However, the dynamical separation, analogous to the Born-Oppenheimer approximation for electrons and nuclei, is irrelevant for strong hydrogen bonds with OH stretching at low frequency. Therefore, by analogy with the seminal case of potassium hydrogen maleate [19], we assume that the effective potential function for the proton can be decomposed into a deep and narrow well containing the “bonding” ground state and a shallow quasi harmonic potential for “non-bonding” excited states. Then, the relative intensities of the components can be ascribed to a substantial shift of the minimum of the upper shallow curve with respect to the centre of the hydrogen bond. With this model, the best fitting potential function to the observed spectral profiles of the K derivative is presented in Fig. 6 and Table 10. The fitting potential for the Cs derivative should be virtually the same. The details of the numerical calculations are given in the Appendix (see below).

We have limited the number of adjustable parameters in the potential function to the number of observed transitions. Since relative intensities were also included in the model, the number of experimental values exceeds the number of parameters. The potential function was decomposed into a narrow gaussian well with a depth of  $\approx 1000$  cm<sup>-1</sup> and a rather flat harmonic potential whose fundamental frequency corresponds to the mean level-spacing. The linear term displacing the upper wave functions with respect to the ground state allows for adjustment of relative intensities. The small cubic term accounts for deviations from harmonicity of the upper potential.

The maximum difference between observed and calculated frequencies in Table 10 is  $\Delta\nu/\nu \approx 2\%$ . The agreement between observed and calculated intensities is less satisfactory, with deviations as large as  $\approx 30\%$ . These differences emphasize the limits of the model that ignores the complex interactions between  $\nu$  OH and  $\delta$  CF<sub>3</sub> modes. Let us recall that the incoherent scattering cross section of fluorine atoms is negligible and the coherent cross section is rather modest ( $\approx 4$  barns), compared to the incoherent cross section for H atoms ( $\approx 80$  barns) [34]. Therefore, INS intensities for the CF<sub>3</sub> modes are almost totally borrowed from the OH mode, thanks to vibrational coupling [24]. Consequently, the estimated frequencies and intensities obtained by simple decomposition into gaussian components presented in Tables 8 and 9 are different from what they should be in the absence of such interactions. We did not try to model this complex interaction. Nevertheless, we consider that coupling with CF<sub>3</sub> modes should not alter the main features of the potential function.

The potential function represented in Fig. 6 is totally unconventional and we are not aware of any other reported example with similar shape. Although this is a particular fit with a chosen analytical function, we consider that any

alternative parameterization should yield basically the same overall shape for the best fit to the observed data.

The potential asymmetry is not in conflict with the centrosymmetric dimers in the crystal structure. At low temperature, only the ground state is populated. The minimum is located at the center of the hydrogen bond and the wave function is virtually symmetrical. At room temperature, the population of excited states ( $\lesssim 5\%$ ) is too small to be distinguished with neutron diffraction. The crystal structure averaged over space and time remains centrosymmetric and the tiny contribution of excited states is embedded in the temperature factors.

In the ground state, the proton is well localized at the centre of the hydrogen bond. The estimated vibrational mean square amplitude of  $\approx 0.02 \text{ \AA}^2$  compares quite favorably to the temperature factors given in Tables 4 and 7. In the excited states, proton transfer to one of the oxygen atoms breaks down the symmetry of the hydrogen bond. The mean position at  $\approx 1 \text{ \AA}$  from the centre is clearly incompatible with the hydrogen bond length  $R_{O\dots O} \approx 2.4 \text{ \AA}$  when the proton is in the ground state. Such a large displacement of the hydrogen atom is possible if the hydrogen bond is broken in the excited states and the spatial extension of the wave functions over several  $\text{\AA}$ , greater than the  $O\dots O$  distance at equilibrium, is representative of the dissociation of the salt.

The hydrogen bistrifluoroacetate complex in the OH excited state is tentatively represented in Fig. 7. The proton is transferred to one of the two entities. The extension of the wave functions suggests that there is a complex combination of translation along the hydrogen bond and rotation around the C—OH bond. At the same time, there may be some twisting around the C—C bond to keep the proton close to the  $O\dots O$  direction. These complex dynamics are possible because the upper level spacing of  $\approx 100 \text{ cm}^{-1}$  is comparable to the frequency of the torsional mode [24]. Proton dynamics on the one hand, internal and  $O\dots H\dots O$  modes at low frequency, on the other, are on the same timescale and can interact strongly.

The asymmetry of the potential in Fig. 6 contrasts to the symmetric potential for potassium hydrogen maleate [19]. Presumably, the electronic structure of the hydrogen maleate ring preserves the symmetry in the excited states. In contrast to the naive representation of the dissociated excited state proposed in Fig 10 of Ref. [19], the excited state should be better regarded as a quantum superposition of the two configurations corresponding to proton transferred to one oxygen atom or the other.

The effective potential functions discussed above were determined upon the assumption of a bare proton,  $m = 1 \text{ amu}$ , while coupling with heavy atoms were ignored. This approximation is reasonable only for the ground state. For



upper states, we should include dynamical coupling with internal degrees of freedom of the trifluoroacetate entities, according to the scheme in Fig. 7. Then, the effective oscillator mass should be significantly greater than 1 amu, the effective upper potential should be steeper than shown in Fig. 6 and the spatial extension of the wave functions should be diminished. The modelling of the effective mass requires more information than available at the present stage of investigation. However, we suspect the overall shape should remain qualitatively the same.

Our conclusions are quite at variance from those proposed in a recent study of the crystal structure of 4-cyano-2,2,6,6-tetramethyl-3,5-heptanedione, a new example of a very short symmetric intramolecular hydrogen bond with  $R_{O...O} = 2.393 \text{ \AA}$  at 100 K [35]. The assignment of the  $\nu$  OH mode to an INS band at  $370 \text{ cm}^{-1}$  is sustained by density functional calculations and magic angle spinning (MAS) solid-state NMR. The authors conclude (surprisingly) that the potential for the hydrogen bonding proton should be of the low-barrier double minimum type, “Although the neutron [diffraction] data better fit a single anisotropic thermal ellipsoid...” Unfortunately, there is no quantitative information on the thermal factors of the proton for comparison with other systems and visual examination does not reveal any significant difference compared to maleate or trifluoroacetates. Clearly, there is not enough information to conclude on the shape of the potential.

## Conclusion

The crystal structures of K and Cs hydrogen bistrifluoroacetates determined with the single crystal neutron diffraction technique confirm that the very short hydrogen bonds linking trifluoroacetate entities are symmetrical at room temperature and at 20 K or 14 K. There is no evidence for proton disorder or phase transition. Any double minimum potential for the proton can be rejected [24].

The complex INS spectral profiles for the OH stretching modes are tentatively decomposed into gaussian components. Comparison with Raman spectra allows us to distinguish bands arising from the  $\delta$   $\text{CF}_3$  modes in the same frequency range. We can thus assign several OH stretching transitions and propose a best fitting potential largely inspired by that previously determined for potassium hydrogen maleate [19]. This potential is composed of a narrow well at the hydrogen bond centre containing the bonding ground state and a rather flat quasiharmonic upper part corresponding to non bonding states. The rather low energy dissociation of this strong hydrogen bond is similar to that observed previously for potassium hydrogen maleate. Apparently, it is a property of this type of hydrogen bonding, rather than a consequence of the

particular structure of the maleate ring.

In contrast to potassium hydrogen maleate, symmetry breakdown occurs for hydrogen bistrifluoroacetates upon excitation of the  $\nu$  OH modes. We conclude that the proton is transferred to one oxygen atom or the other. Presumably, the preserved potential symmetry of the hydrogen maleate in the excited states is a consequence of the particular structure of the ring. The excited states should be regarded as quantum superposition of proton transferred to the two oxygen atoms of the hydrogen bond.

We conclude that the concept of hydrogen bonding for the ground state and hydrogen nonbonding for excited states could be of general relevance for strong symmetric hydrogen bonds.

### Appendix: Calculation of energy levels, wave functions and INS intensities

The variational method is the most appropriate to determine analytical potential functions fitting any given energy level scheme. The expansion of the eigen functions with harmonic basis sets allows us to calculate all matrix elements of interest for vibrational spectroscopy. In this appendix we gather the formulae to resolve the Schrödinger equation for a dimensionless particle with effective mass  $m^*$  experiencing a potential  $V(x)$  along the  $x$  coordinate:

$$-\frac{\hbar^2}{2m^*} \frac{d^2\Psi}{dx^2} + V(x)\Psi = E\Psi \quad (1)$$

with

$$V(x) = V_p(x) + V_G(x) = \sum_{l=1}^6 v_l x^l + \sum_{l=1}^3 a_l \exp(-b_l x^2), \quad (2)$$

where  $V_p$  is the polynomial potential and  $V_G$  the sum of three Gaussians, to allow for a rich variety of potential forms. We also propose a straightforward method to test the accuracy of the eigenfunctions.

In order to construct a basis set, let  $\omega_0/(2\pi)$  be a frequency and consider the dimensionless variables  $\xi = \alpha x$ , with  $\alpha = \sqrt{m\omega_0/\hbar}$ ,  $\tilde{V} = V/(\hbar\omega_0)$  and  $\tilde{E} = E/(\hbar\omega_0)$ . Then

$$\tilde{V}_p = \sum_{l=1}^6 \tilde{v}_l \xi^l,$$

with

$$\tilde{v}_l = v_l / (\hbar \omega_0 \alpha^l)$$

Here, the scaled energies are such that the difference between energy levels of the harmonic oscillator is 1 instead of 4 in Ref. [36]. Our constants  $v_l$ , divided by a factor of 2 compared to [36] are such that the potential energy of the harmonic oscillator  $\tilde{V} = \xi^2/2$  corresponds to  $\tilde{v}_l = 1/2 \delta_{l,2}$  (where  $\delta_{l,2}$  is the Kronecker symbol). This choice of scaling sounds more natural and clear. Then,  $\alpha = \alpha_0 \sqrt{\tilde{\nu}_0 m^*}$  can be expressed in  $\text{\AA}^{-1}$  units with  $\alpha_0 = 0.17273$  and  $\tilde{\nu}_0 = \omega_0 / (2 \pi c)$  in  $\text{cm}^{-1}$  units.

In the new variables Eq. (1) reads:

$$\hat{h} \psi = -\frac{1}{2} \frac{d^2 \psi}{d \xi^2} + \tilde{V} \psi = \tilde{E} \psi, \quad (3)$$

with  $\psi = \sqrt{\alpha} \Psi$  normalized with respect to  $\xi$ .

For a harmonic oscillator the normalized solutions of Eq. 3 are:

$$u_n(\xi) = (2^n n! \sqrt{\pi})^{-1/2} H_n(\xi) \exp(-\xi^2/2) \quad n = 0, 1, \dots, \quad (4)$$

$\{H_n\}$  being the Hermite polynomials. The functions  $\{u_n\}$  form a suitable orthonormal basis set for localized solutions  $\psi$ . For numerical calculations the dimension  $N$  of the basis has to be finite. We found  $N = 60$  is suitable to calculate the 10 lowest energy levels with good accuracy (see below). The matrix elements of  $\hat{h}$  in Eq. 3 are:

$$\hat{h}_{n,m} = \langle n | \hat{h} | m \rangle = \int_{-\infty}^{\infty} u_n(\xi) \hat{h} u_m(\xi) d \xi.$$

The matrix elements used to calculate the eigenstates for a given oscillator mass and a sixth order polynomial potential or a Gaussian potential can be found in Refs. [36] and [37], respectively. As these papers may be nowadays difficult to obtain, we present the algorithms in condensed form, with an alternative definition of the scaling factors for the polynomial form.

For the polynomial potential  $V = V_p$  we obtain:

$$\begin{aligned}
\hat{h}_{n,n}^p &= (n + \frac{1}{2}) (\frac{1}{2} + \tilde{v}_2) + \frac{3}{4} (2n^2 + 2n + 1) \tilde{v}_4 \\
&\quad + \frac{1}{8} (20n^3 + 30n^2 + 40n + 15) \tilde{v}_6 ; \\
\hat{h}_{n,n-1}^p &= \frac{1}{2} \sqrt{2n} (\tilde{v}_1 + \frac{3}{2} n \tilde{v}_3 + \frac{5}{4} (2n^2 + 1) \tilde{v}_5) ; \\
\hat{h}_{n,n-2}^p &= \frac{1}{2} \sqrt{n(n-1)} \left( -\frac{1}{2} + \tilde{v}_2 + (2n-1) \tilde{v}_4 \right. \\
&\quad \left. + \frac{15}{4} (n^2 - n - 1) \tilde{v}_6 \right) ; \\
\hat{h}_{n,n-3}^p &= \frac{1}{2} \sqrt{\frac{n(n-1)(n-2)}{2}} (\tilde{v}_3 + \frac{5}{2} (n-1) \tilde{v}_5) ; \\
\hat{h}_{n,n-4}^p &= \frac{1}{4} \sqrt{n(n-1)(n-2)(n-3)} \left( \tilde{v}_4 + \frac{3}{4} (2n-3) \tilde{v}_6 \right) ; \\
\hat{h}_{n,n-5}^p &= \frac{1}{4} \sqrt{\frac{n(n-1)(n-2)(n-3)(n-4)}{2}} \tilde{v}_5 ; \\
\hat{h}_{n,n-6}^p &= \frac{1}{8} \sqrt{n(n-1)(n-2)(n-3)(n-4)(n-5)} \tilde{v}_6 .
\end{aligned} \tag{5}$$

The terms independent on  $\tilde{v}_l$  arise from the kinetic energy. All other matrix elements are zero except for the symmetric ones  $\hat{h}_{n-l,n}^p = \hat{h}_{n,n-l}^p$ ,  $l = 1, \dots, 6$ .

For a Gaussian potential term  $W = a \exp(-bx^2)$ , the scaled potential is  $\tilde{W} = \tilde{a} \exp(-\tilde{b} \xi^2)$ , with  $\tilde{a} = a/(\hbar \omega_0)$  and  $\tilde{b} = b/\alpha^2$ . Matrix elements  $\hat{W}_{n,m}$  in the subset  $\{u_n\}_{n=0}^{N-1}$  are calculated according to Ref. [37]: construct a  $(N, 2N-1)$  auxiliary matrix  $\hat{G}$  with an iterative procedure. The first row is calculated as:

$$\hat{G}_{0,m} = \sqrt{\frac{m!}{2^m(1+\tilde{b})}} \frac{(-\theta)^{m/2}}{(m/2)!} \quad \text{for } m \text{ (even)}=0, \dots, 2N-1, \tag{6}$$

with  $\theta = \tilde{b}/(1+\tilde{b})$ . The second row is calculated as:

$$\hat{G}_{1,m} = \sqrt{m} \hat{G}_{0,m-1} + \sqrt{m+1} \hat{G}_{0,m+1} \quad ; \text{ for } m \text{ (odd)}=1, \dots, 2N-2 \tag{7}$$

Each successive row of index  $n$  ( $2 \leq n \leq N-1$ ) depends on the two previous ones as:

$$\begin{aligned}
\hat{G}_{n,m} &= 1/\sqrt{n} (\sqrt{m} \hat{G}_{n-1,m-1} + \sqrt{m+1} \hat{G}_{n-1,m+1} - \sqrt{n-1} \hat{G}_{n-2,m}); \\
m &= n, n+2, n+4, \dots, 2N-n-1
\end{aligned}$$

All elements not explicitly assigned are set to zero. Let us redefine  $\hat{G}$  as the  $(N, N)$  square matrix corresponding to its first  $N$  columns. The procedure above has led to an upper triangular matrix. The elements of the lower triangle are obtained by symmetry  $\hat{G}(n, m) = \hat{G}(m, n)$ , for all  $n, m$  such that  $m < n$ . The  $(N, N)$  matrix corresponding to  $\tilde{W}$  is  $\hat{W} = \tilde{a} \hat{G}(\tilde{b})$ .

Therefore, the matrix  $\hat{h}$  corresponding to the full potential  $V$  in Eq. 2 is:

$$\hat{h} = \hat{h}^p + \sum_{l=1}^3 \tilde{a}_l \hat{G}(\tilde{b}_l)$$

If  $\{\tilde{E}_n\}_{n=0}^{N-1}$  are eigenvalues in increasing order, and  $\hat{C}$  is the  $(N, N)$  matrix whose column  $n$  is the normalized eigenvector corresponding to  $\tilde{E}_n$ , the eigenfunctions are

$$\psi_n(\xi) = \sum_{m=0}^{N-1} \hat{C}_{n,m} u_m(\xi).$$

The eigenvalues and eigenfunctions in physical units are

$$E_n = \hbar \omega_0 \tilde{E}_n$$

and

$$\Psi_n(x) = \sqrt{\alpha} \sum_{m=0}^{N-1} \hat{C}_{n,m} u_m(\alpha x).$$

The eigenfunctions  $\Psi_n$  are analytical functions (although with numerically calculated coefficients) composed of a polynomial of order  $N - 1$  multiplied by a Gaussian. Therefore, derivatives are easily obtained and the accuracy of the solutions can be checked by substitution in Eq. (1). As a rule of thumb, the last coefficients of each series  $\{\hat{C}_{n,m}\}_{m=0}^{N-1}$  (say, the last 10 for  $N = 60$ ) have to be very small with respect to the largest of the others. This is generally achieved for the first few eigenfunctions to be compared with observation.

The parameter  $\omega_0$  largely determines whether the truncated expansions of  $\{\Psi_n\}$  are good approximations. As a rule of thumb the exponential in Eq. 4 should be small (say  $\sim e^{-2}$ ) at the estimated limits for the the particle position. This leads to  $\omega_0 \approx 16 \hbar / (m^* \Delta x^2)$ , where  $\Delta x$  is the width of the classically allowed region, or  $\tilde{\nu}_0 \approx 16 / (m^* \alpha_0^2 \Delta x^2)$  with  $\tilde{\nu}_0$  and  $\Delta x$  in  $\text{cm}^{-1}$  and  $\text{\AA}$  units, respectively. For a single minimum this is obtained if  $\hbar \omega_0$  is close to the first observed transition. In this case, basis sets limited to sizes  $N \approx 40$  are convenient. For potentials composed of a narrow well and a shallow upper part, like those for strong symmetric hydrogen bonds under consideration in this paper, it is necessary to increase the size to  $N = 60$ . The accuracy for the 10 lower eigenvalues is far beyond experimental errors and the accuracy of the eigenvectors is better than 1%. Further increment of  $N$  is unnecessary as numerical errors become larger the higher powers of  $x$ .

The INS intensity for a transition  $|0\rangle \rightarrow |n\rangle$  at energy  $E_n$  is proportional to the scattering function

$$S(Q, E) = |\langle 0 | \exp(-iQx) | n \rangle|^2 \delta(E - E_n).$$

For a spectrometer like TFXA [38], energy and momentum transfer,  $E$  and  $Q$ , respectively, are correlated as

$$E \approx \frac{h^2 Q^2}{16.759 m^*},$$

with  $E$  and  $Q$  in  $\text{cm}^{-1}$  and  $\text{\AA}^{-1}$  units, respectively.

Therefore, for a given set of parameters  $\{v_l\}$ ,  $\{a_l\}$ ,  $\{b_l\}$  and  $\omega_0$ , we are able to obtain the frequencies and intensities of the first few transitions with good accuracy. Using standard numerical methods it is possible to determine the values of the parameters that best fit the observed frequencies and intensities.

## References

- [1] A. N. Baker, *J. Chem. Phys.* 22 (1954) 1625.
- [2] G. Pimentel, C. McClellan, A. Lester, *The hydrogen bond*, W.H. Freeman, San Francisco, 1960.
- [3] S. N. Vinogradov, R. H. Linnell, *Hydrogen Bonding*, Van Nostrand-Reinhold, New York, 1971.
- [4] R. Janoschek, Vol. 1 of *The Hydrogen Bond*, recent developments in theory and experiments, P. Schuster, G. Zundel and C. Sandorfy ed., North-Holland, Amsterdam, 1976, p. 165, and references cited therein.
- [5] E. Matsushita, T. Matsubara, *Prog. Theoret. Phys.* 67 (1982) 1.
- [6] A. Novak, *Struct. and Bonding (Berlin)* 18 (1974) 177.
- [7] W. W. Cleland, *Biochemistry* 31 (1992) 317.
- [8] W. W. Cleland, M. M. Kreevoy, *Science* 264 (1994) 1887.
- [9] S. F. Darlow, W. Cochram, *Acta Cryst.* 14 (1961) 1250.
- [10] S. F. Darlow, *Acta Cryst.* 14 (1961) 121257.
- [11] H. M. E. Cardwell, J. D. Dunitz, L. E. Orgel, *J. Chem. Soc.* (1953) 3740.
- [12] K. Nakamoto, Y. A. Sarma, G. T. Behnke, *J. Chem. Phys.* 42 (1965) 1662.
- [13] F. Avbelj, B. Orel, M. Klanjek, D. Hadzi, *Spectrochim. Acta* 41 A (1985) 75.
- [14] H. R. Zelsmann, Z. Mielke, M. M. Ilczyszyn, *Spectrochim. Acta* 44 A (1988) 705.
- [15] M. M. Ilczyszyn, J. Baran, H. Ratajczak, A. J. Barnes, *J. Mol. Struct.* 270 (1992) 499.

- [16] J. Tomkinson, I. J. Braid, J. Howard, T. C. Waddington, *Chem. Phys.* 64 (1982) 151.
- [17] J. Howard, J. Tomkinson, J. Eckert, J. A. Goldstone, A. D. Taylor, *J. Chem. Phys.* 78 (1983) 3150.
- [18] J. Tomkinson, J. Penfold, J. Howard, *J. Mol. Struct.* 142 (1986) 1.
- [19] F. Fillaux, N. Leygue, J. Tomkinson, A. Cousson, W. Paulus, Structure and dynamics of the symmetric hydrogen bond in potassium hydrogen maleate: a neutron scattering study., *Chem. Phys.* 244 (1999) 387–403.
- [20] C. C. Wilson, L. H. Thomas, C. A. Morrison, A symmetric hydrogen bond revisited: potassium hydrogen maleate by variable temperature, variable pressure neutron diffraction and plane-wave dft methods, *Chem. Phys. letters* 381 (2003) 102–108.
- [21] F. Fillaux, A. Cousson, J. Tomkinson, Comment on: “a symmetric hydrogen bond revisited: potassium hydrogen maleate by variable temperature, variable pressure neutron diffraction and plane-wave dft methods” [*chem. phys. letters* 381 (2003) 102], *Chem. Phys. Letters*, submitted.
- [22] L. Golic, J. C. Speakman, The crystal structures of the acid salts of some monobasic acids. part x. potassium, rubidium and cesium hydrogen ditrifluoroacetates, *J. Chem. Soc.* (1965) 2530–2542.
- [23] D. Hadži, B. Orel, A. Novak, Infrared and raman spectra of some acid salts containing crystallographically symmetric hydrogen bonds, *Spectrochimica Acta* 29A (1973) 1745–1753.
- [24] F. Fillaux, J. Tomkinson, Proton-transfer dynamics in the hydrogen bond. inelastic neutron scattering, infrared and raman spectra of  $\text{KH}(\text{CF}_3\text{COO})_2$  and  $\text{CsH}(\text{CF}_3\text{COO})_2$ , *Chem. Phys.* 158 (1991) 113–127.
- [25] J. C. Evans, *Spectrochim. Acta* 16 (1960) 994.
- [26] J. C. Evans, *Spectrochim. Acta* 18 (1962) 507.
- [27] U. Fano, *Nuovo Cimento* 12 (1935) 156.
- [28] [www-llb.cea.fr](http://www-llb.cea.fr).
- [29] P. W. Betteridge, J. R. Carruthers, R. I. Cooper, C. K. Prout, D. J. Watkin, Crystals. issue 11, *J. Appl. Cryst.* 36 (2003) 1487.
- [30] B. I. Stepanov, *Nature* (1946) 157.
- [31] Y. Maréchal, A. Witkowski, *J. Chem. Phys.* 48 (1968) 3697.
- [32] P. Schuster, G. Zundel, C. Sandorfy, The hydrogen bond. Recent developments in theory and experiments, Vol. I, II and III, North-Holland Pub. Co., Amsterdam, 1976.

- [33] G. L. Hofacker, Y. Maréchal, M. A. Ratner, Dynamical properties of hydrogen bonded systems, Vol. 1 of The hydrogen bond Recent developments in theory and experiments, North-Holland, Amsterdam, 1976, Ch. 6, pp. 295–357.
- [34] A.-J. Dianoux, G. Lander, Neutron Data Booklet, ILL neutrons for science, 2002.
- [35] J. A. Belot, J. Clark, J. A. Cowan, G. S. Habison, A. I. Kolesnikov, Y. sik Kye, A. J. Schultz, C. Silvernail, X. Zhao, The shortest symmetrical O—H···O hydrogen bond has a low-barrier double-well potential, *J. Phys. Chem. B* 108 (2004) 6922–6926.
- [36] E. Heilbronner, H. Rutishauser, F. Gerson, Verfahren zur programmgesteuerten Berechnung der Eigenwerte eindimensionaler Molekel-Modelle, *Sch. Chem. G. XLII-VII* (249) (1959) 2285–2303.
- [37] S. Y. Chan, D. Stelman, Oscillators perturbed by Gaussian barriers, *Jou. Chem. Phys.* 39 (3) (1963) 545–551.
- [38] <http://www.isis.rl.ac.uk/molecularSpectroscopy/tfxa/index.htm>.



Table 1

Neutron single crystal diffraction data and structure refinement for potassium and cesium hydrogen bistrifluoroacetates.  $\lambda = 0.8305 \text{ \AA}$ . Space groups monoclinic  $I2/a$  for potassium and  $A2/a$  for cesium. Both with  $Z = 4$ . The criterion for observed reflections was  $I > 3\sigma(I)$ . The variance for the last digit is given in parentheses.

	KH(CF <sub>3</sub> COO) <sub>2</sub>		CsH(CF <sub>3</sub> COO) <sub>2</sub>	
	20K	298 K	14 K	298 K
a (Å)	8.68(1)	8.78(1)	13.44(1)	13.623(8)
b (Å)	10.023(9)	10.18(1)	4.942(9)	5.033(3)
c (Å)	9.146(9)	9.28(1)	14.35(1)	14.741(6)
$\beta$ (°)	100.36(8)	99.96(9)	112.88(9)	112.46(9)
V (Å <sup>3</sup> )	782.6	817.0	878.4	934.0
$D_x$ (Mg m <sup>-3</sup> )	2.259	2.164	2.722	2.559
Measured reflections	1979	2164	3476	3897
Independent reflections	1769	1472	1977	2096
and observed reflections	1503	1142	1557	1062
$R_{int}$	0.037	0.038	0.048	0.064
Refinement on	F	F	F	F
R-factor	0.040	0.045	0.0399	0.043
Weighted R-factor	0.042	0.029	0.0345	0.040
Goodness of fit	1.070	1.088	1.049	1.079
Number of reflections	1503	1142	1557	1062
Number of parameters	76	76	76	76
used in refinement				
Extinction coefficient	22.7(7)	17.2(8)	10.0(3)	11.2(9)

Table 2

Atomic positions and isotropic temperature factors for  $\text{KH}(\text{CF}_3\text{COO})_2$  at 20 K (first lines) and 298 K (second lines). The variance for the last digit is given in parentheses.

Atom	$x/a$	$y/b$	$z/c$	U(iso)( $\text{\AA}^2$ )
K(1)	0.2500	0.47035(13)	1.0000	0.0022
	0.2500	0.4691(2)	1.0000	0.0306
C(1)	0.08108(6)	0.65992(5)	0.61071(5)	0.0020
	0.0771(1)	0.66238(9)	0.61201(9)	0.0306
C(2)	-0.04133(6)	0.66059(5)	0.71503(6)	0.0020
	-0.04356(9)	0.66241(8)	0.71512(8)	0.0260
O(1)	-0.02359(7)	0.58604(6)	0.82262(7)	0.0040
	-0.02706(13)	0.58871(11)	0.81966(11)	0.0333
O(2)	-0.15042(7)	0.74496(6)	0.67180(7)	0.0045
	-0.15011(14)	0.74556(14)	0.67428(14)	0.0426
F(1)	0.15118(7)	0.78039(7)	0.61351(7)	0.0050
	0.14415(18)	0.78021(15)	0.61321(18)	0.0519
F(2)	0.19203(7)	0.56895(7)	0.65128(7)	0.0046
	0.18745(15)	0.57426(17)	0.65321(17)	0.0490
F(3)	0.01440(8)	0.63619(7)	0.47010(7)	0.0046
	0.01325(19)	0.63720(16)	0.47512(13)	0.0474
H(1)	-0.2500	0.7500	0.7500	0.0166
	-0.2500	0.7500	0.7500	0.0574

Table 3

Interatomic distances in Å units and angles in degrees in  $\text{KH}(\text{CF}_3\text{COO})_2$  at 20 K (first lines) and 298 K (second lines). The variance for the last digit is given in parentheses.

C(1)–C(2)	1.5504(17)	C(1)–F(1)	1.3503(15)
	1.5455(19)		1.335(2)
C(1)–F(2)	1.3296(16)	C(1)–F(3)	1.3332(17)
	1.327(2)		1.322(2)
C(2)–O(1)	1.2230(15)	C(2)–O(2)	1.2779(16)
	1.2148(18)		1.270(2)
O(2)–H(1)	1.2179(13)	C(2)–C(1) - F(1)	109.9(1)
	1.2159(17)		110.08(14)
C(2)–C(1) - F(2)	111.9(1)	C(2)–C(1) -F(3)	111.57(11)
	111.51(14)		111.87(13)
F(1)–C(1) - F(2)	107.86(12)	F(1)–C(1)–F(3)	107.08(11)
	107.78(17)		107.18(16)
F(2)–C(1) - F(3)	108.29(11)	C(1)–C(2)–O(1)	119.4(1)
	108.24(16)		119.61(12)
C(1)–C(2)–O(2)	111.4(1)	O(1)–C(2)–O(2)	129.21(9)
	111.36(13)		129.03(12)
C(2)–O(2)–H(1)	114.2(1)	O(2)–H(1)–O(2)	180.0(1)
	114.87(13)		180.0(1)

Table 4

Thermal parameters in  $\text{\AA}^2$  units for  $\text{KH}(\text{CF}_3\text{COO})_2$  at 20 K (first lines) and 298 K (second lines). The variance for the last digit is given in parentheses.

Atom	$U_{11}$	$U_{22}$	$U_{33}$	$U_{23}$	$U_{13}$	$U_{12}$
K(1)	0.0027(4)	0.0018(4)	0.0020(4)	0.0000	0.0003(3)	0.0000
	0.035(1)	0.0263(8)	0.0325(9)	0.0000	0.0122(7)	0.0000
C(1)	0.00117(19)	0.00268(19)	0.0023(2)	0.00024(13)	0.00039(14)	0.00003(13)
	0.0297(4)	0.0329(4)	0.0299(3)	0.0029(3)	0.0078(3)	-0.0022(3)
C(2)	0.00157(19)	0.00238(19)	0.0023(2)	0.00055(14)	0.00060(14)	0.00064(13)
	0.0258(3)	0.0272(3)	0.0249(3)	0.0045(3)	0.0043(2)	0.0005(3)
O(1)	0.0038(2)	0.0048(2)	0.0035(2)	0.00241(17)	0.00120(17)	0.00108(15)
	0.0360(5)	0.0341(4)	0.0307(4)	0.0115(4)	0.0088(3)	0.0042(4)
O(2)	0.0033(2)	0.0060(2)	0.0047(2)	0.00268(17)	0.00194(17)	0.00312(16)
	0.0376(5)	0.0507(7)	0.0418(5)	0.0194(5)	0.0129(4)	0.0180(4)
F(1)	0.0049(2)	0.0048(2)	0.0054(2)	0.00042(18)	0.00072(18)	-0.00222(17)
	0.0523(8)	0.0457(7)	0.0597(8)	0.0074(6)	0.0150(6)	-0.0195(6)
F(2)	0.0027(2)	0.0054(2)	0.0057(2)	0.00058(18)	0.00076(18)	0.00219(17)
	0.0353(6)	0.0579(8)	0.0557(7)	0.0057(6)	0.0135(5)	0.0141(5)
F(3)	0.0054(2)	0.0057(2)	0.0025(2)	-0.00028(17)	0.00020(17)	-0.00006(17)
	0.0608(8)	0.0535(7)	0.0285(5)	-0.0032(5)	0.0094(5)	0.0005(6)
H(1)	0.0177(7)	0.0158(8)	0.0160(7)	0.0034(6)	0.0023(6)	0.0029(6)
	0.0539(17)	0.0577(18)	0.0582(17)	0.0199(15)	0.0034(13)	0.0152(14)

Table 5

Atomic positions and isotropic temperature factors for CsH(CF<sub>3</sub>COO)<sub>2</sub> at 14 K (first lines) and 298 K (second lines). The variance for the last digit is given in parentheses.

Atom	$x/a$	$y/b$	$z/c$	U(iso)(Å <sup>2</sup> )
Cs(1)	-0.2500	0.21541(18)	0.0000	0.0013
	-0.2500	0.2170(4)	0.0000	0.0377
F(1)	-0.01883(5)	0.61975(15)	0.15253(5)	0.0059
	-0.01376(14)	0.5971(4)	0.15586(14)	0.0652
F(2)	0.10983(5)	0.39738(15)	0.26553(5)	0.0069
	0.11435(18)	0.3806(5)	0.26110(12)	0.0761
F(3)	0.14684(5)	0.72718(14)	0.18559(5)	0.0063
	0.14651(17)	0.7048(4)	0.18308(15)	0.0722
O(1)	0.16871(5)	0.28677(13)	0.08444(5)	0.0050
	0.16517(9)	0.2837(3)	0.0796(1)	0.0445
O(2)	-0.00501(5)	0.18925(14)	0.05235(5)	0.0045
	-0.00336(8)	0.1803(3)	0.0543(1)	0.0442
C(1)	0.07995(4)	0.52050(11)	0.17554(4)	0.0031
	0.08238(8)	0.5005(2)	0.17453(7)	0.0401
C(2)	0.08431(4)	0.31424(11)	0.09597(4)	0.0027
	0.08415(6)	0.30433(18)	0.09498(7)	0.0312
H(1)	0.0000	0.0000	0.0000	0.0166
	0.0000	0.0000	0.0000	0.0592

Table 6

Interatomic distances in Å units and angles in degrees in CsH(CF<sub>3</sub>COO)<sub>2</sub> at 20 K (first lines) and 298 K (second lines). The variance for the last digit is given in parentheses.

C(1)–C(2)	1.549(3)	C(1)–F(1)	1.331(3)
	1.5403(14)		1.3236(19)
C(1)–F(2)	1.340(3)	C(1)–F(3)	1.331(2)
	1.326(2)		1.324(2)
C(2)–O(1)	1.216(3)	C(2)–O(2)	1.277(3)
	1.2132(13)		1.2746(13)
O(2)–H(1)	1.218(2)	C(2)–C(1)–F(1)	112.3(2)
	1.2221(12)		112.3(1)
C(2)–C(1)–F(2)	109.20(17)	C(2)–C(1)–F(3)	111.56(15)
	110.24(13)		111.63(11)
F(1)–C(1)–F(2)	107.6(2)	F(1)–C(1)–F(3)	108.10(12)
	107.61(15)		107.41(16)
F(2)–C(1)–F(3)	107.9(2)	C(1)–C(2)–O(1)	118.59(17)
	107.44(16)		118.5(1)
C(1)–C(2)–O(2)	112.5(2)	O(1)–C(2)–O(2)	128.92(15)
	112.86(8)		128.62(11)
C(2)–O(2)–H(1)	114.03(19)	O(2)–H(1)–O(2)	180.0(1)
	114.18(9)		180.0(1)

Table 7

Thermal parameters in  $\text{\AA}^2$  units for  $\text{CsH}(\text{CF}_3\text{COO})_2$  at 14 K (first lines) and 298 K (second lines). The variance for the last digit is given in parentheses.

Atom	$U_{11}$	$U_{22}$	$U_{33}$	$U_{23}$	$U_{13}$	$U_{12}$
Cs(1)	0.0009(3)	0.0015(3)	0.0019(3)	0.0000	0.0009(2)	0.0000
	0.0319(6)	0.0359(7)	0.0526(9)	0.0000	0.0244(6)	0.0000
F(1)	0.0048(2)	0.0069(3)	0.0061(2)	-0.00185(18)	0.00239(17)	0.00167(19)
	0.0614(8)	0.069(1)	0.068(1)	-0.0250(8)	0.0275(7)	0.0110(8)
F(2)	0.0095(2)	0.0082(3)	0.0030(2)	0.00077(19)	0.00246(17)	0.0006(2)
	0.0959(13)	0.0907(14)	0.0369(7)	0.0065(8)	0.0199(8)	0.0014(12)
F(3)	0.0074(2)	0.0047(3)	0.0068(3)	-0.00216(19)	0.00288(18)	-0.00294(18)
	0.0837(12)	0.0581(9)	0.0777(12)	-0.0291(9)	0.0342(9)	-0.0324(9)
O(1)	0.0038(2)	0.0055(2)	0.0071(2)	-0.00185(18)	0.00373(16)	-0.00097(18)
	0.0344(5)	0.0458(6)	0.0592(7)	-0.0061(6)	0.0245(5)	-0.0035(5)
O(2)	0.0029(2)	0.0039(2)	0.0068(2)	-0.00313(18)	0.00219(16)	-0.00094(17)
	0.0305(4)	0.0407(6)	0.0634(7)	-0.0202(6)	0.0202(5)	-0.0076(4)
C(1)	0.00369(17)	0.0030(2)	0.00295(18)	-0.00084(14)	0.00151(13)	0.00004(15)
	0.0448(5)	0.0407(5)	0.0346(4)	-0.0067(4)	0.0148(3)	-0.0051(4)
C(2)	0.00267(18)	0.00290(19)	0.00315(18)	-0.00089(15)	0.00183(13)	-0.00025(14)
	0.0285(3)	0.0284(3)	0.0370(4)	-0.0012(3)	0.0130(3)	-0.0011(3)
H(1)	0.0131(6)	0.0176(8)	0.0185(7)	0.0006(7)	0.0053(5)	-0.0011(6)
	0.0403(13)	0.0498(16)	0.088(2)	-0.0059(17)	0.0247(14)	-0.0011(12)

Table 8

Gaussian decomposition of the INS spectrum of  $\text{KH}(\text{CF}_3\text{COO})_2$  in the OH stretching region (see Fig. 5).

Peak	Width $\text{cm}^{-1}$	Gravity center $\text{cm}^{-1}$	Area %	Assignment
1	12	527	1.9	$\delta \text{CF}_3$
2	36	560	3.4	$\delta \text{CF}_3$
3	18	602	4.4	OH stretching
4	36	648	5.1	$\delta \text{CF}_3$
5	41	704	17.9	OH stretching
6	22	750	5.0	$\delta \text{CF}_3$
7	20	774	5.0	$\delta \text{CF}_3$
8	38	799	18.1	OH stretching
9	78	871	27.6	OH stretching, $\delta \text{CF}_3$
10	73	955	10.9	OH stretching
11	18	1033	0.8	OH stretching

Table 9

Gaussian decomposition of the INS spectrum of  $\text{CsH}(\text{CF}_3\text{COO})_2$  in the OH stretching region (see Fig. 5).

Peak	Width $\text{cm}^{-1}$	Gravity center $\text{cm}^{-1}$	Area %	Assignment
1	12	523	1.8	$\delta \text{CF}_3$
2	19	550	1.5	$\delta \text{CF}_3$
3	20	597	3.9	OH stretching
4	26	647	2.6	$\delta \text{CF}_3$
5	38	704	14.2	OH stretching
6	27	751	4.7	$\delta \text{CF}_3$
7	57	798	30.6	OH stretching
8	23	849	5.1	$\delta \text{CF}_3$
9	53	880	20.1	OH stretching
10	68	950	13.4	OH stretching
11	55	1043	2.0	OH stretching



Table 10

Observed and calculated INS OH stretching frequencies and intensities for  $\text{KH}(\text{CF}_3\text{COO})_2$ . The calculated ones correspond to the potential  $V = -185.074x + 122.598x^2 - 10.506x^3 - 1232.04 \exp(-28.149x^2)$ ,  $V$  and  $x$  in  $\text{cm}^{-1}$  and  $\text{\AA}$ , respectively. For the TFXA spectrometer used in Ref. [24], energy and momentum transfer are correlated as  $\tilde{\nu} = Q^2/(16.759m)$  with  $\tilde{\nu}$ ,  $Q$  and  $m$  in  $\text{cm}^{-1}$ ,  $\text{\AA}^{-1}$  and amu units, respectively. au: arbitrary units.

Transitions	Observations			Calculations		
	freq. ( $\text{cm}^{-1}$ )	Q ( $\text{\AA}^{-1}$ )	int. (au)	freq. ( $\text{cm}^{-1}$ )	Q ( $\text{\AA}^{-1}$ )	int. (au)
$0 \rightarrow 1$	601	6.0	0.25	614	6.1	0.38
$0 \rightarrow 2$	703	6.5	0.96	701	6.5	0.93
$0 \rightarrow 3$	798	6.9	1.00	787	6.9	1.00
$0 \rightarrow 4$	870	7.2	0.76	872	7.2	0.59
$0 \rightarrow 5$	956	7.6	0.58	953	7.5	0.37

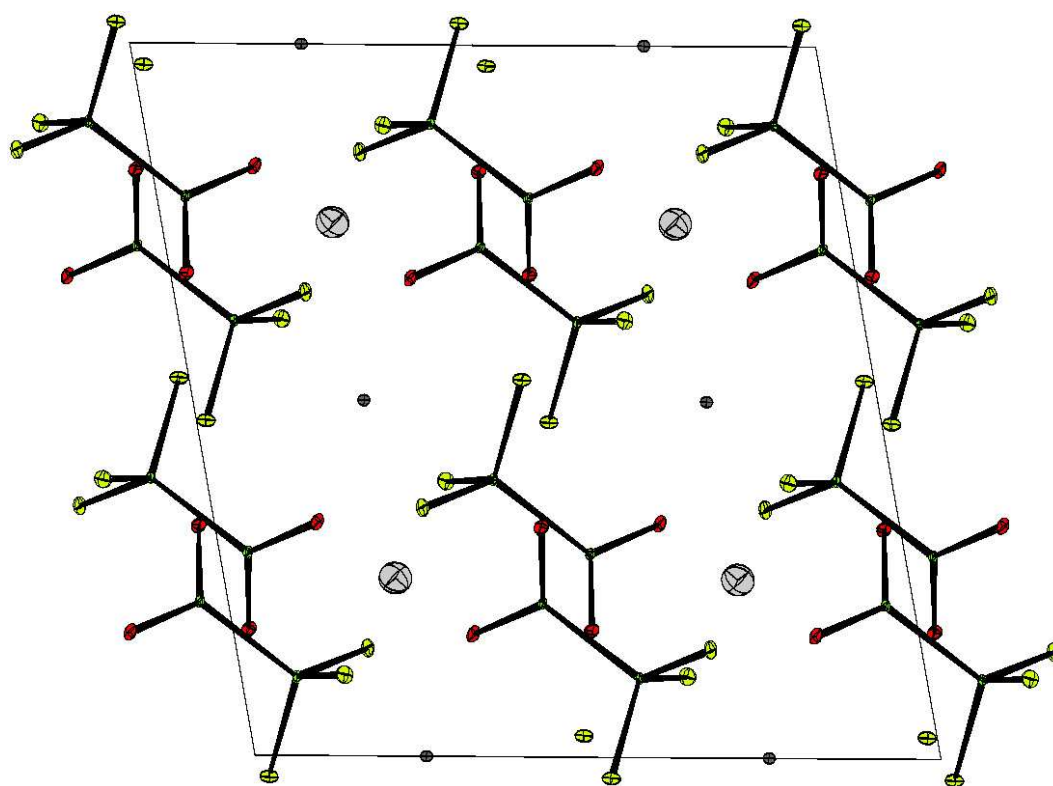


Fig. 1. Projection of the crystal structure of potassium hydrogen bistrifluoroacetate at 20 K onto the  $(a, c)$  plane and thermal ellipsoids for atoms.

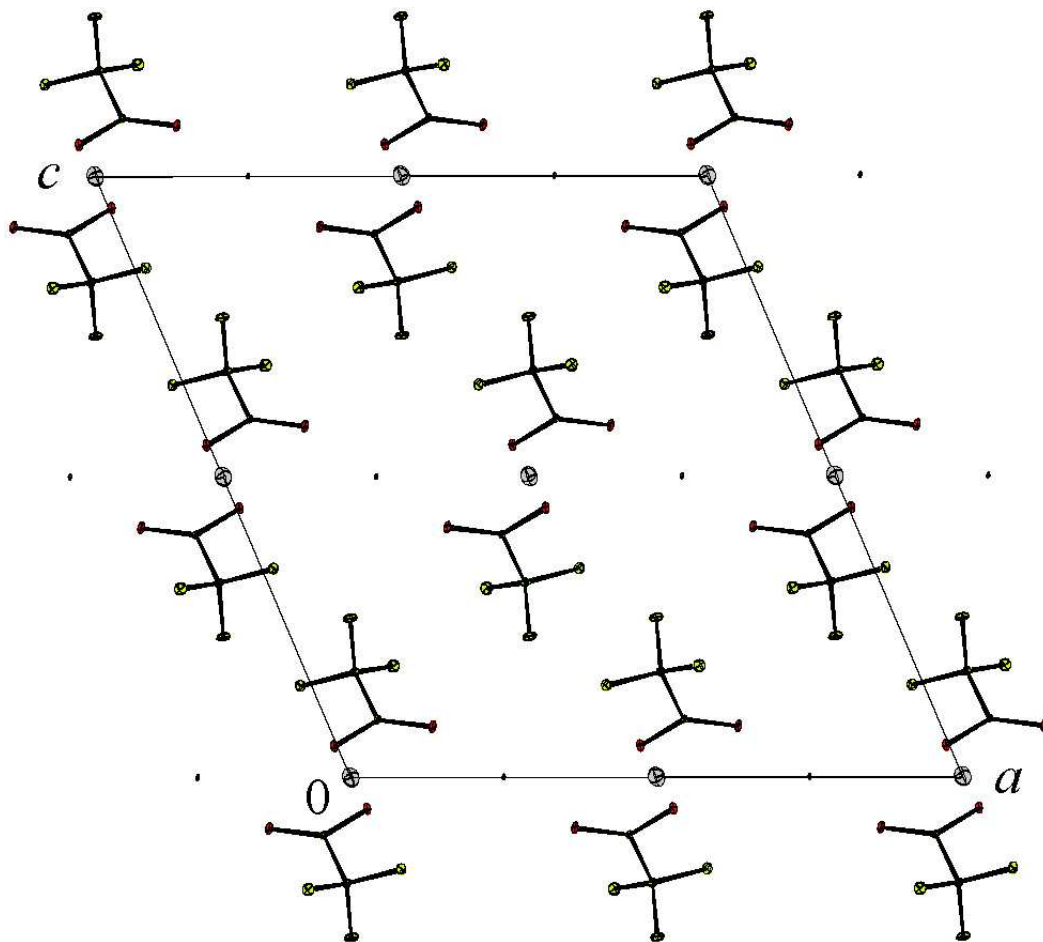


Fig. 2. Projection of the crystal structure of cesium hydrogen bistrifluoroacetate at 14 K onto the  $(a, c)$  plane and thermal ellipsoids for atoms.

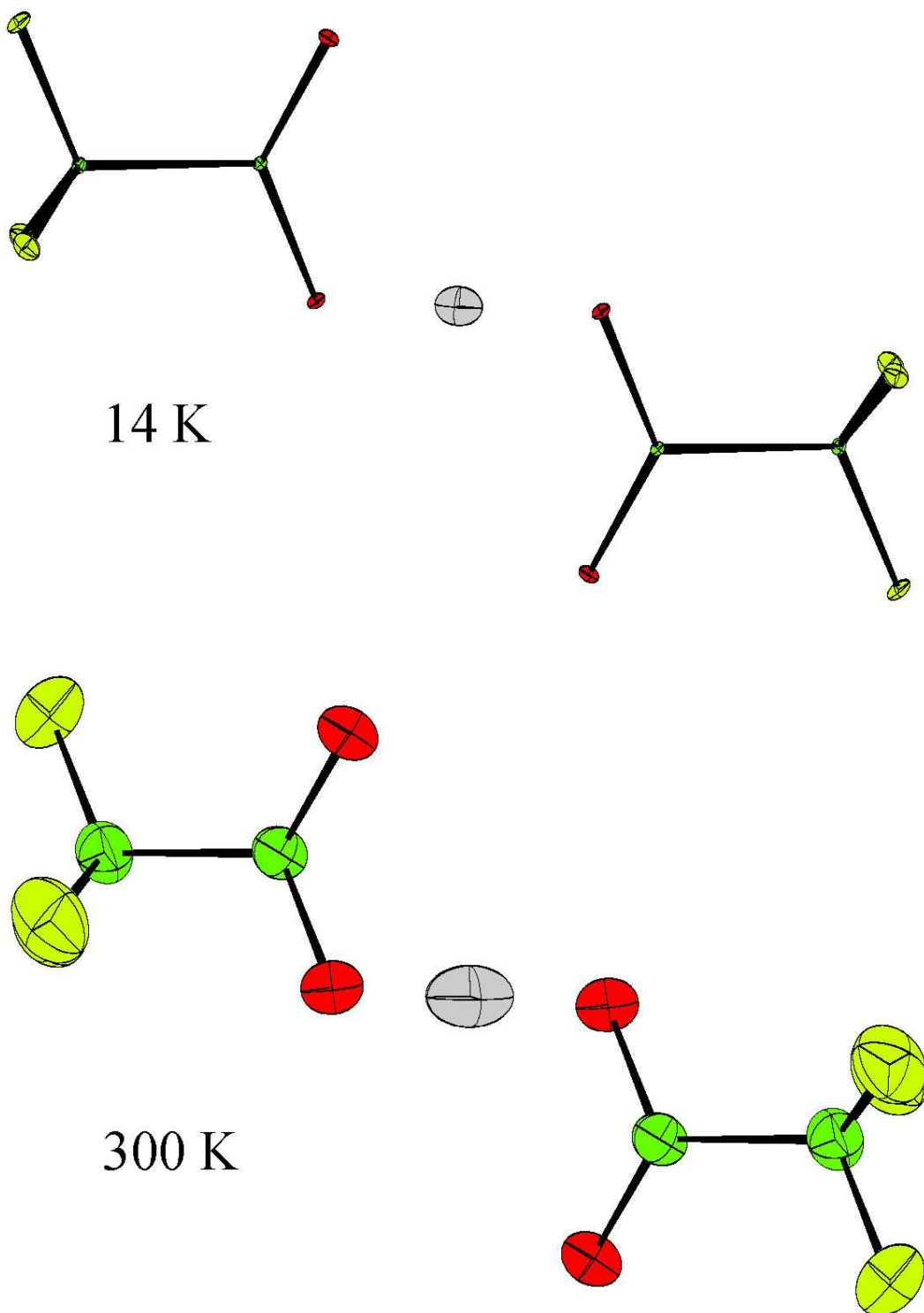


Fig. 3. Comparison of the hydrogen bistrifluoroacetate entities and thermal ellipsoids for atoms of the potassium salt at 20 and 300 K. Right: projection onto the mean-plane of the carboxylic entities. Left: view along the hydrogen bond direction.

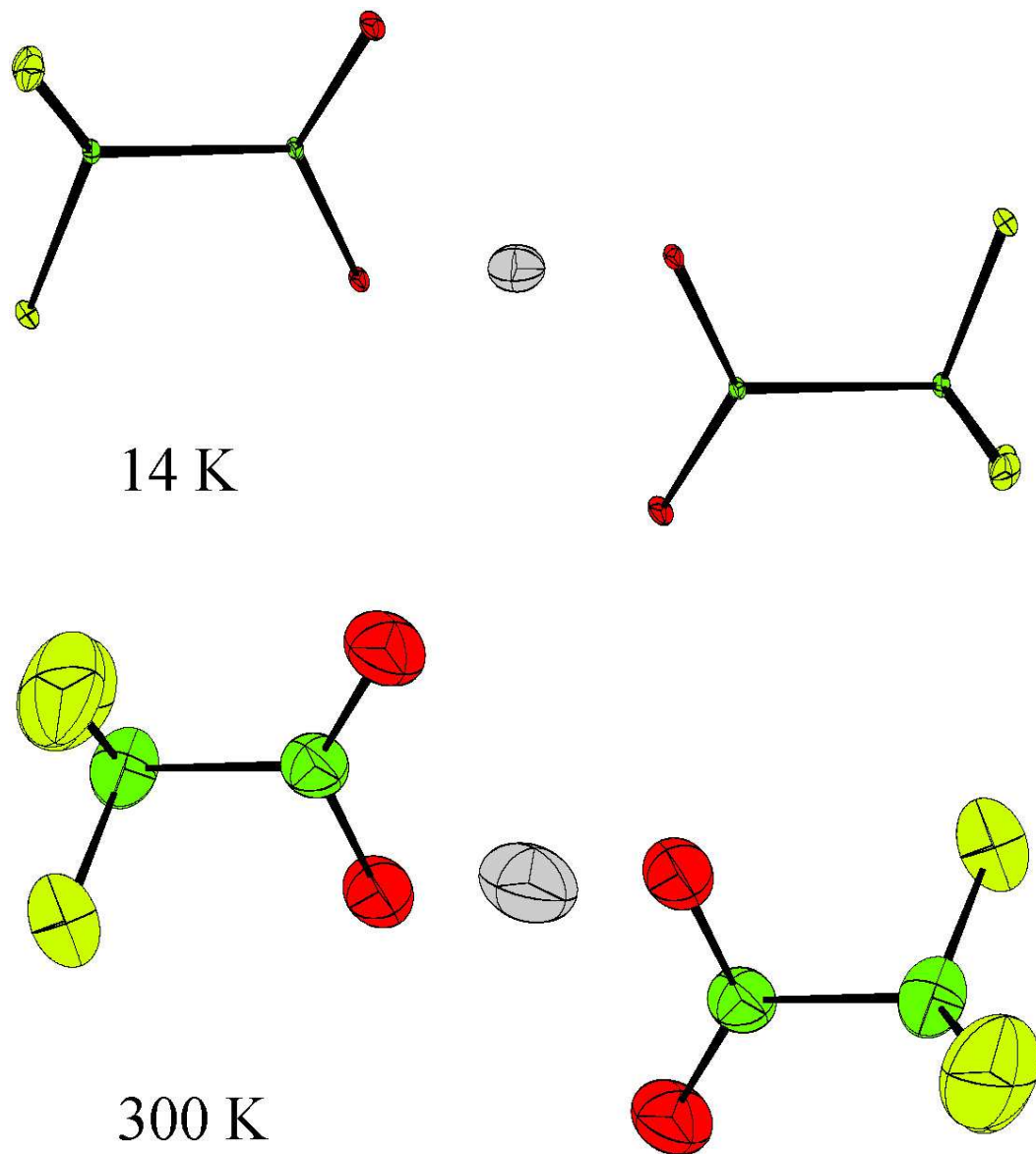


Fig. 4. Comparison of the hydrogen bistrifluoroacetate entities and thermal ellipsoids for atoms of the cesium salt at 14 and 300 K. Right: projection onto the mean-plane of the carboxylic entities. Left: view along the hydrogen bond direction.

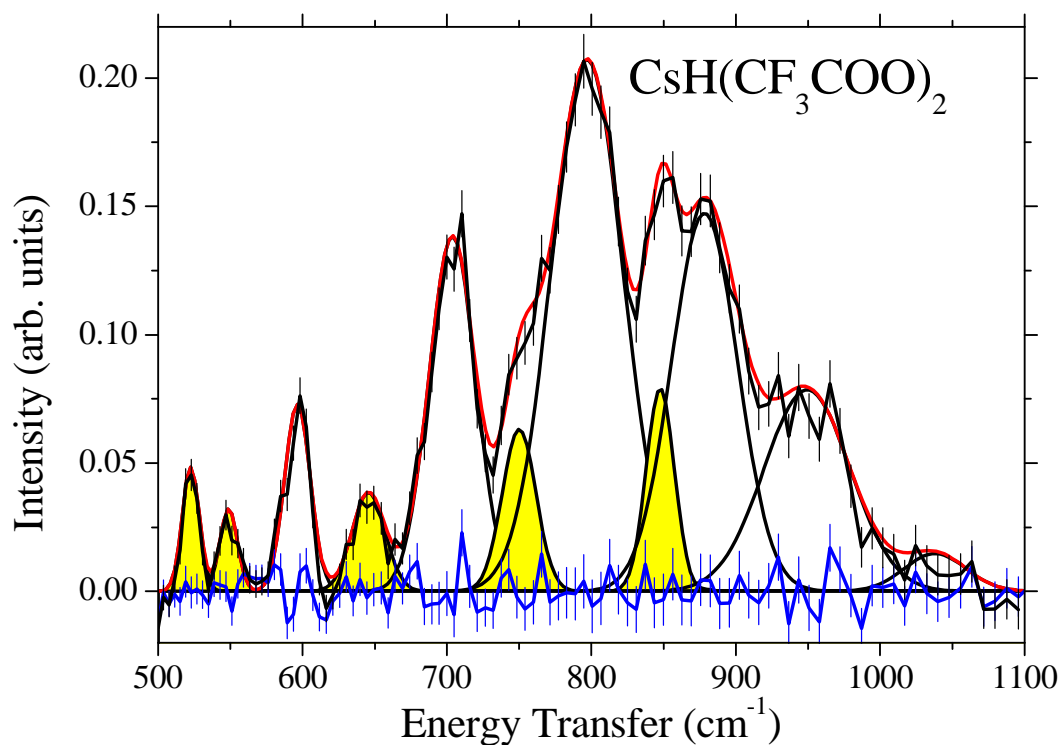
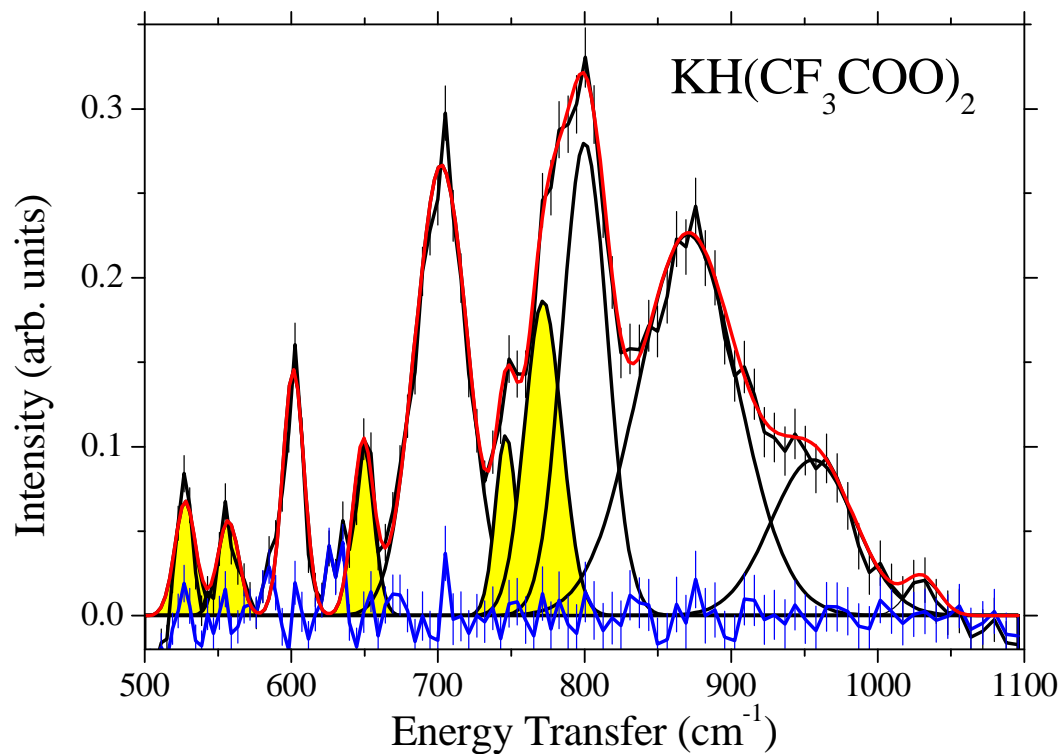


Fig. 5. Inelastic neutron scattering spectra and band decomposition into gaussian profiles in the OH stretching region of  $\text{KH}(\text{CF}_3\text{COO})_2$  and  $\text{CsH}(\text{CF}_3\text{COO})_2$  at 20 K. The filled components are attributed to other modes (see text). The residual of the fit is compared to the error bars.

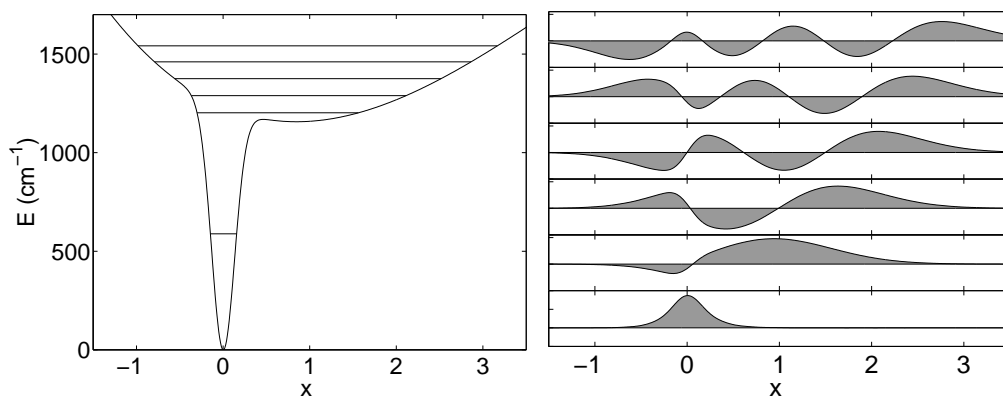


Fig. 6. Left: Calculated potential and energy levels for  $\text{KH}(\text{CF}_3\text{COO})_2$ .  $V = -185.074x + 122.598x^2 - 10.506x^3 - 1232.04\exp(-28.149x^2)$ , with  $V$  and  $x$  in  $\text{cm}^{-1}$  and  $\text{\AA}$  units, respectively. Right: The corresponding wave functions,  $x$  in  $\text{\AA}$  units.

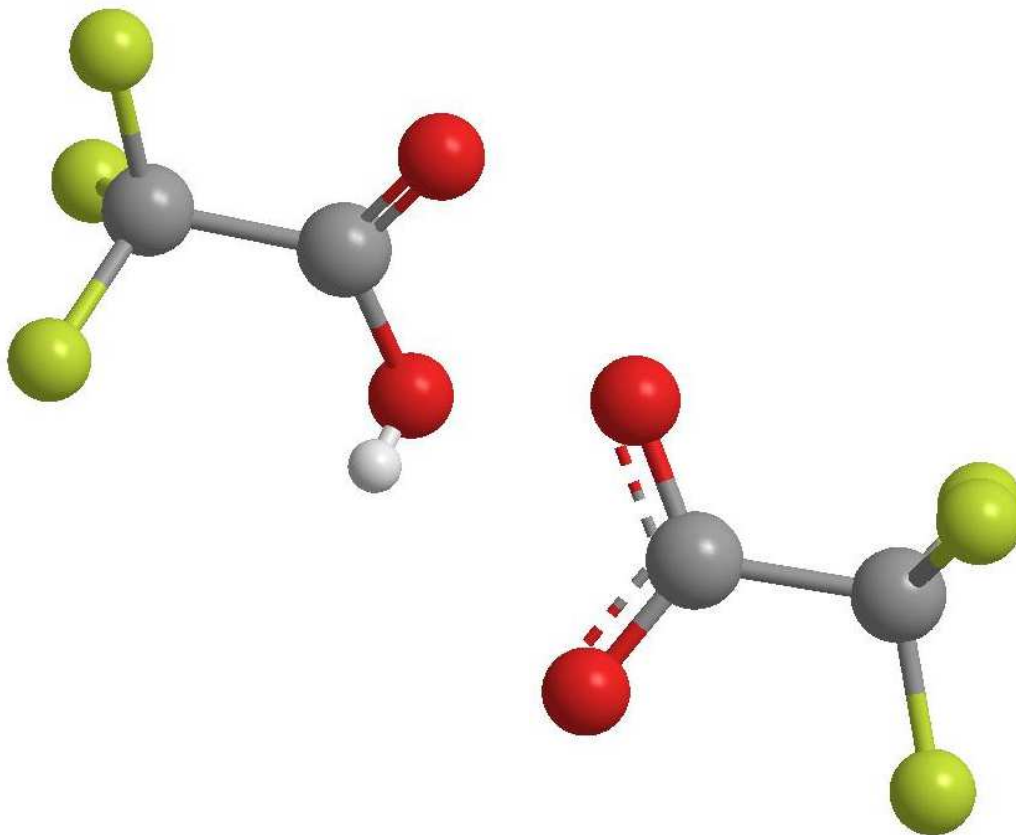


Fig. 7. Artistic view of the dissociation of the hydrogen bistrifluoroacetate ion in the OH stretching excited state